Accurate pH and O_2 Measurements from Spray Underwater Gliders

YUICHIRO TAKESHITA,[a] BRENT D. JONES,[a] KENNETH S. JOHNSON,[a] FRANCISCO P. CHAVEZ,[b] DANIEL L. RUDNICK,[b] MARGUERITE BLUM,[a] KYLE CONNER,[c] SCOTT JENSEN,[a] JACQUELINE S. LONG,[a] THOM MAUGHAN,[a] KEATON L. MERTZ,[a] JEFFREY T. SHERMAN,[b] AND JOSEPH K. WARREN[a]

[a] *Monterey Bay Aquarium Research Institute, Moss Landing, California*
[b] *Scripps Institution of Oceanography, University of California, San Diego, La Jolla, California*
[c] *Department of Oceanography, University of Hawai'i at Mānoa, Honolulu, Hawaii*

(Manuscript received 25 June 2020, in final form 15 October 2020)

ABSTRACT: The California Current System is thought to be particularly vulnerable to ocean acidification, yet pH remains chronically undersampled along this coast, limiting our ability to assess the impacts of ocean acidification. To address this observational gap, we integrated the Deep-Sea-DuraFET, a solid-state pH sensor, onto a Spray underwater glider. Over the course of a year starting in April 2019, we conducted seven missions in central California that spanned 161 glider days and >1600 dives to a maximum depth of 1000 m. The sensor accuracy was estimated to be ± 0.01 based on comparisons to discrete samples taken alongside the glider (n = 105), and the precision was ±0.0016. CO_2 partial pressure, dissolved inorganic carbon, and aragonite saturation state could be estimated from the pH data with uncertainty better than ± 2.5%, ± 8 μmol kg^{-1}, and ± 2%, respectively. The sensor was stable to ±0.01 for the first 9 months but exhibited a drift of 0.015 during the last mission. The drift was correctable using a piecewise linear regression based on a reference pH field at 450 m estimated from published global empirical algorithms. These algorithms require accurate O_2 as inputs; thus, protocols for a simple predeployment air calibration that achieved accuracy of better than 1% were implemented. The glider observations revealed upwelling of undersaturated waters with respect to aragonite to within 5 m below the surface near Monterey Bay. These observations highlight the importance of persistent observations through autonomous platforms in highly dynamic coastal environments.

KEYWORDS: Ocean; In situ oceanic observations; Instrumentation/sensors; Profilers, oceanic

1. Introduction

The California Current System (CCS) is a hot spot for ocean acidification (Hauri et al. 2009), and studies suggest that it is experiencing rapid ocean acidification (Gruber et al. 2012; Osborne et al. 2020), which could severely reduce habitats for organisms that are sensitive to elevated CO_2 levels. For example, a meta-analysis for species group in the CCS revealed that 26 out of 34 functional groups responded negatively to higher CO_2 levels (Busch and McElhany 2016), including commercially important organisms such as Dungeness crab (Miller et al. 2016), pink shrimp (Dupont et al. 2014), and bivalves (Barton et al. 2012). There is evidence that ocean acidification is already having observable impacts through widespread mortality of Pacific oyster *Crassostrea gigas* (Barton et al. 2012, 2015) and severe shell dissolution of pteropod *Limacina helicina* (an important source of food for salmon, cod, herring, and mackerel) (Bednaršek et al. 2014). Survival of these pteropods also seems to be affected by exposure history to high CO_2 levels over the course of several weeks (Bednaršek et al. 2017), indicating the importance of observing and modeling carbonate chemistry at high spatiotemporal resolution. Despite these potential socioeconomic consequences from ocean acidification, we still have a poor understanding of the drivers that determine the spatial structure of pH along the CCS over weekly (episodic upwelling), seasonal, and interannual (e.g., El Niño) time scales. This makes it difficult to accurately assess and track the impacts of ocean acidification in the CCS. Monitoring efforts for ocean acidification have increased (McLaughlin et al. 2015), however, most of these monitoring sites are shore based and provide high temporal resolution but limited spatial context, particularly in offshore waters where high spatial variability in pH has been documented (Chavez and Messié 2009).

Underwater gliders are an effective platform to collect sustained, depth-resolved high resolution data, particularly in the coastal ocean (Rudnick 2016). Glider observations typically are made on spatiotemporal scales of hours and kilometers or better, allowing them to resolve mesoscale (Martin et al. 2009) and submesoscale (Rudnick and Cole 2011) processes. Furthermore, they can capture seasonal to interannual or decadal variability by occupying repeated transects over time. For example, Spray gliders operating in the California Underwater Glider Network (CUGN) have made sustained observations along three lines in the CCS since 2007 (Rudnick et al. 2017) and have been used to study the impacts of the 2014–15 marine heat wave (Zaba and Rudnick 2016) and the El Niño of 2015–16 (Jacox et al. 2016). Glider observations are also particularly useful for constraining data assimilating models, and it has been demonstrated that assimilating glider data can significantly improve model forecasting capabilities (Pasmans et al. 2019). Biogeochemical sensors have been

Denotes content that is immediately available upon publication as open access.

Supplemental information related to this paper is available at the Journals Online website: https://doi.org/10.1175/JTECH-D-20-0095.s1.

Corresponding author: Yuichiro Takeshita, yui@mbari.org

DOI: 10.1175/JTECH-D-20-0095.1

© 2021 American Meteorological Society. For information regarding reuse of this content and general copyright information, consult the AMS Copyright Policy (www.ametsoc.org/PUBSReuseLicenses).
Brought to you by NOAA Central Library | Unauthenticated | Downloaded 08/13/24 07:32 PM UTC

equipped onto gliders to measure parameters such as O_2 (Pierce et al. 2012), nitrate (Evans et al. 2013; Vincent et al. 2018), bio-optics (Briggs et al. 2011), and zooplankton (Ohman et al. 2019). However, examples of pH sensors on gliders are still rare. Adding pH measurements to gliders operating in the CUGN would be particularly useful for capturing the high spatiotemporal variability in pH (Chavez et al. 2017), which would significantly improve our ability to assess vulnerability and impacts of ocean acidification as well as improve data assimilative models in the CCS (Mattern et al. 2017; Moore et al. 2017).

The Deep-Sea-DuraFET (DSD) is a potentiometric pH sensor that consists of a Honeywell Ion Sensitive Field Effect Transistor (ISFET) die and a Cl-Ion Selective Electrode (Cl-ISE) as the reference electrode exposed directly to seawater, which are housed in a pressure tolerant package (Johnson et al. 2016). This solid-state sensor has been demonstrated to have excellent stability and performance in seawater (Martz et al. 2010) and is a proven technology capable of autonomous deployments for years (Johnson et al. 2017). Currently over 180 biogeochemical profiling floats equipped with DSD pH sensors have been deployed, mostly operating in the Southern Ocean. The fleetwide accuracy of the pH from these floats after implementing a robust and documented quality control (QC) protocol is 0.005 ± 0.013 (Johnson et al. 2017). The quality of data from profiling floats is sufficient to resolve annual air–sea CO_2 fluxes (Gray et al. 2018; Bushinsky et al. 2019) and seasonal cycles of derived carbonate parameters such as saturation state (Ω) and pCO_2 (Takeshita et al. 2018; Williams et al. 2018). However, the DSD was initially developed for profiling floats, and DSD payloads for gliders are not widely available for the community.

pH sensors have been operated on underwater gliders previously. For example, an ISFET and Cl-ISE pH sensor was operated in the Mediterranean Sea on a Seaglider for 12 days down to a depth of 1000 m (Hemming et al. 2017). This ISFET was not manufactured by Honeywell and was described as a custom-built "experimental" ISFET (Shitashima 2010; Shitashima et al. 2013). This system exhibited large sensor drift, and corrections were made post deployment for temperature and pressure effects. Nonetheless, they were able to document spatiotemporal pH variability in the Sardinian Sea for this prototype deployment. More recently, a modified DSD was successfully operated on a Slocum glider for deployments lasting weeks (Saba et al. 2019). This system utilized the same sensing elements as the DSD (i.e., Honeywell ISFET and Cl-ISE), but the sensing elements were integrated into a glider CTD payload that is specific to Slocum gliders. As a result, this design is not easily adaptable for other underwater glider types, thus an alternative design is required for other glider types such as Spray (Sherman et al. 2001) and Seagliders (Eriksen et al. 2001).

Here, we present results from operating the DSD pH sensor on a Spray underwater glider over a year starting in April 2019 (Fig. 1). Seven deployments were conducted in the central CCS near Monterey Bay for a total of 161 glider days, and over 1600 dives to depths of up to 1000 m. Sensor accuracy and performance were assessed by comparing glider data to full water column discrete samples taken alongside the glider. The stability of the pH sensor was assessed by comparison to a deep reference pH field estimated from published global empirical algorithms. Accurate O_2 data are required as an input for the algorithms. Thus, protocols for achieving accurate O_2 measurements through predeployment air calibration and correction for slow response time errors without amplifying sensor noise are also presented.

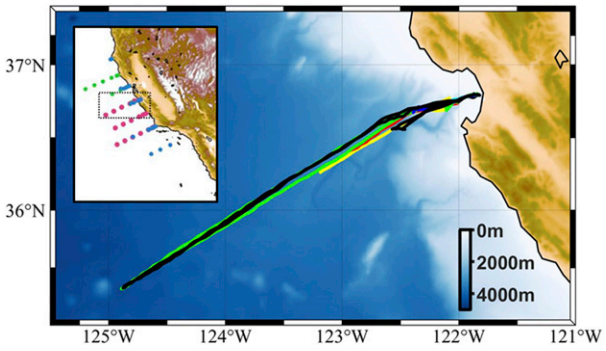

FIG. 1. The main map shows deployment tracks over seven missions conducted since April 2019. The offshore transects follow CalCOFI line 67. Different color lines represent separate missions. The color scale indicates bottom depth. The inset shows the larger study region, and the colored circles represent hydrography stations used to assess the empirical algorithms. Colors correspond to different cruises and are consistent with Fig. 3. Dashed box shows the domain for the main map.

2. Methods

a. Integration of the DSD onto Spray

Spray is an underwater glider that is approximately 50 kg and 2 m in length (Sherman et al. 2001). The Spray hull consists of an aluminum pressure case that houses the battery packs, hydraulic system, compass, attitude sensor, and the microprocessor controller. All scientific sensors are in the flooded aft bay, where the external bladders are located. Spray profiles vertically in the water column by adjusting its buoyancy by pumping oil into, or out of an external bladder. The wings of the vehicle provide lift, allowing it to travel horizontally at approximately 20–30 cm s^{-1}. Spray is capable of profiling to 1000 m, which takes approximately 6 h, and transits 6 km horizontally per profile. Spray is typically programmed to collect data only on ascent to conserve energy and to obtain the lowest sensor noise levels (Davis et al. 2008). Spray ascends at a rate of approximately 0.1 m s^{-1}, and sensors are polled every 8 s. This produces measurements with vertical resolution slightly better than 1 m. Once at the surface, Spray rolls 90° to expose the antenna located in its wings to transmit data, receive commands, and obtain a navigational fix. A typical Spray deployment can last between 3 and 5 months, depending on profiling depth, sensor suite, and profiling interval. Clark electrode O_2 sensors have been operated on Sprays (Ohman et al. 2013), and more recently, O_2 optodes [Sea-Bird Electronics, Inc., (SBE) model 63] have been routinely operated on Sprays for several years.

Brought to you by NOAA Central Library | Unauthenticated | Downloaded 08/13/24 07:32 PM UTC

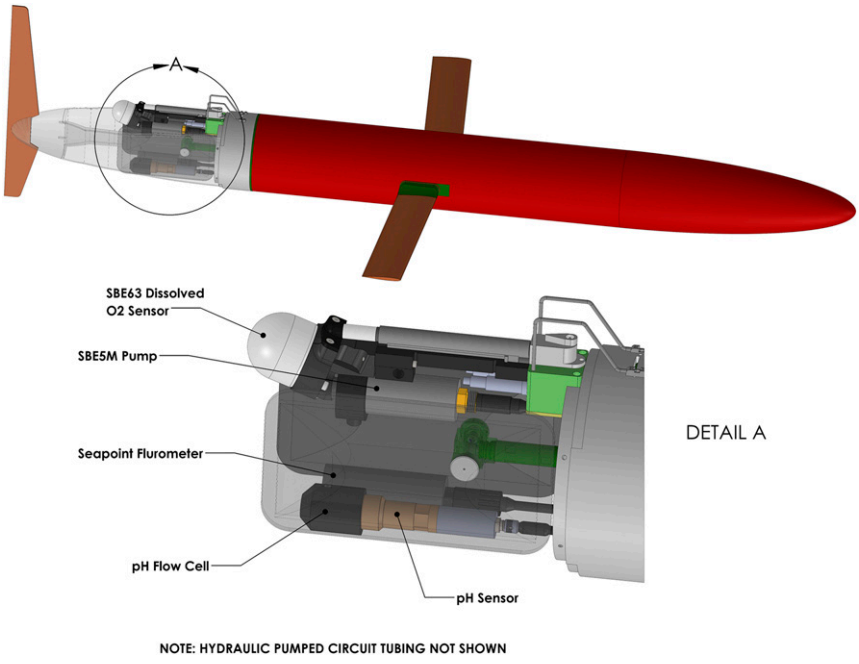

FIG. 2. Schematic drawing of a Spray glider equipped with a DSD pH sensor. Detail A shows the sensor configuration in the flooded aft sensor bay.

The DSD electrode was operated using custom electronics designed at the Monterey Bay Aquarium Research Institute (MBARI), updated based on the controller utilized on profiling floats (Johnson et al. 2016). The ISFET circuitry was powered with a dedicated battery, starting at least 1 week before deployment to allow sufficient time for the ISFET to warm up, which typically takes several days. The pH controller was powered using the main glider battery and communicated with the glider controller using RS232. Each pH measurement takes approximately 1 Hz, consuming ~0.5 J. This allowed it to be polled within the regular 8-s cycle and represents <2% of the overall power budget. The DSD electrode was placed in the flooded aft bay (Fig. 2) and connected to the pH controller that was placed in the pressure housing through an IE55 rubber molded cable.

The DSD electrode was purchased from Sea-Bird Scientific, where pressure and temperature coefficients were determined following protocols outlined in Johnson et al. (2016). The constant term of the reference potential (k_0) is specific to each electrode and electronics pair, thus the k_0 was determined in the laboratory prior to the first deployment using the same pH controller that was installed into the glider. The electrode was conditioned in natural, flowing seawater for 2 weeks prior to determining k_0 so that the reference electrode was fully equilibrated with respect to bromide ion in seawater (Bresnahan et al. 2014). Based on our experience, flowing seawater is important for this equilibration period, as the reference electrode can absorb enough bromide ion to appreciably change its concentration in a recirculating container. The DSD electrode was then operated for ~1 week, and discrete samples for pH were taken twice a day to determine k_0. The estimated uncertainty of k_0 is better than 100 μV, which roughly equates to a pH of ~0.0015. Details for pH calculations for the DSD can be found in Johnson et al. (2016).

The Spray payload for this study included a CTD, an O_2 optode (SBE63), a chlorophyll fluorometer (Seapoint), and a DSD pH electrode, all plumbed into a pumped flow stream. A single Spray glider was used for all missions. An SBE-5SM impeller pump was used to pump seawater at 10 mL s^{-1}. The DSD was plumbed directly downstream of the O_2 sensor (Fig. 2). Integrating the sensor into a pumped flow stream has the benefit of improved sensor response, combating biofouling, and protection from light, as ISFETs are light sensitive (Hemming et al. 2017). A flow cell for the DSD was machined out of black Delrin that could be easily removed to enable access for sensor inspection and cleaning. On one deployment, measurements were made on both the ascent and descent with the same vertical resolution to assess pressure hysteresis and sensor response time errors.

Decimated pH data were sent back to shore in real time with 0.001 resolution, along with diagnostic engineering data to monitor sensor health. Real-time data are depth bin averaged to reduce data transmission time, and full resolution data were downloaded at recovery. Range and spike tests were performed following protocols for pH profiling floats (Johnson et al. 2018). Furthermore, we removed bad data based on visual inspection of the data that was caused by a clogged CTD. To date, the prototype pH sensor has produced >99% ''good'' qualified data. Real-time and quality controlled data are made public through the Central and Northern California Ocean Observing System (CeNCOOS) and the GliderViz data portal operated at MBARI (http://www.mbari.org/gliderviz).

The pH data were assessed for sensor drift once deployed by comparing sensor pH to a reference pH field at 450 m calculated using the Carbonate System and Nutrients Concentration from

Brought to you by NOAA Central Library | Unauthenticated | Downloaded 08/13/24 07:32 PM UTC

Hydrological Properties and Oxygen Using a Neural Network (CANYON-B) algorithm, with temperature, salinity, pressure, oxygen, location, and date as inputs (Bittig et al. 2018b). The estimated uncertainty for CANYON-B pH is ±0.018. This is similar to the approach utilized for profiling floats, except they use a reference pH at deeper depths of 1500 m (Johnson et al. 2017). The depth of 450 m was chosen because the CANYON-B pH agreed best with hydrographic pH data at this depth in this region of the CCS (see section 2c for details). If sensor drift were observed, it could be corrected by adjusting the k_0 as done for profiling floats, and it is assumed that the temperature and pressure coefficients do not change over time (Johnson et al. 2017).

Other carbonate parameters such as pCO_2, dissolved inorganic carbon (DIC), and saturation state with respect to aragonite (Ω_{Ar}) can be derived by combining sensor pH and estimated total alkalinity (TA) from empirical relationships (Takeshita et al. 2015, 2018; Williams et al. 2017, 2018; Saba et al. 2019). Here, we utilized CANYON-B to estimate TA, phosphate, and silicate concentrations (Bittig et al. 2018b) as inputs to CO2SYS (van Heuven et al. 2011) with carbonate equilibrium constants from (Lueker et al. 2000), as recommended for best practices (Dickson et al. 2007). To assess the uncertainty of the derived parameters, we conducted a Monte Carlo error analysis (100 simulations) on data from a monthlong mission in April 2019. For each simulation, normally distributed errors were introduced into pH (±0.01), TA (±6.8 μmol kg^{-1}), and nutrient concentrations (±20%). See sections 2c and 3a for how the uncertainties for TA and pH were determined, respectively. High uncertainty in nutrient concentrations was arbitrarily chosen to represent a worst case scenario, since it has been demonstrated that derived variables are insensitive to nutrient concentrations (Williams et al. 2017). The overall uncertainty was calculated as one standard deviation of the simulations. Note that this uncertainty analysis does not take into account the errors that may be caused from the recently demonstrated internal inconsistency of spectrophotometric pH with the other carbonate parameters (Patsavas et al. 2015; Williams et al. 2017; Carter et al. 2018; Fong and Dickson 2019; Takeshita et al. 2020).

b. Calibration of O_2

Accurate O_2 measurements are a prerequisite for accurately estimating pH using empirical algorithms, as O_2 is an input for these algorithms. Approximately, a 1 μmol kg^{-1} bias in O_2 leads to a 0.0016 bias in the computed algorithm pH at depth (Williams et al. 2016), thus an accuracy of 1% or better is desired (Williams et al. 2017). However, optode O_2 sensors are known to drift exponentially low during storage due to degraded O_2 accessibility to the luminophore (D'Asaro and McNeil 2013; Bittig et al. 2018a) and can lead to biases of −10% to −20% at the time of deployment (Takeshita et al. 2013). Fortunately, drift is minimal once deployed (Johnson et al. 2015; Bittig and Körtzinger 2017). The calibration error due to storage drift can be corrected for by applying a gain correction:

$$O_{2,corr} = G \times O_{2,raw}, \quad (1)$$

where $O_{2,corr}$ is the corrected O_2, G is the gain correction factor, and $O_{2,raw}$ is the raw optode output (Johnson et al. 2015). Optodes can be calibrated by making measurements in air with knowledge of total atmospheric pressure and humidity, since the mole fraction of O_2 in the atmosphere is constant (Bushinsky and Emerson 2013). This approach has been successfully applied in situ on profiling floats (Bittig and Körtzinger 2015; Johnson et al. 2015; Bushinsky et al. 2016) and gliders (Nicholson and Feen 2017) to achieve accuracy of better than 1% at the surface. To utilize this approach in situ, however, the optode must be removed from the pumped flow stream to be exposed to the atmosphere at the surface. Unfortunately, this is not currently possible for SBE63 optodes, as they are designed to be plumbed into a pumped flow stream. Furthermore, removing it from the pumped flow stream will result in larger dynamic errors due to slow sensor response (Bittig et al. 2014; Bittig and Körtzinger 2017), which is not ideal especially along the coast of California where there are persistent, steep oxyclines (Chan et al. 2008).

As an alternative to in situ air calibrations, we conducted air calibrations for the SBE63 optode directly prior to deployment starting on the third mission. Atmospheric air was flushed through the flow cell using an aquarium aeration pump, and the atmospheric pressure and humidity was measured using a barometer (Digi-Sense 68000–49, ±4 mb and ±5% humidity). Air was pumped through the flow cell for at least 30 min before calibration. Once stable sensor readings were verified, five measurements were averaged to calculate G. The temperature reading from the CTD was used for the air calibration. This approach takes advantage of the fact that gliders are frequently recovered, and thus, sensors can be recalibrated as necessary. The predeployment calibration would correct for storage drift, if detected. This simplified air calibration setup can achieve an accuracy of 1%, based on a series of experiments, which are summarized in the supplementary materials. Since no systematic changes in G was observed, we used the mean G to calibrate O_2 for all missions.

The slow response time of oxygen optodes can cause errors, especially in regions with a high oxygen gradient (Takeshita et al. 2013; Bittig et al. 2014). The response time (τ) is dependent on the flow rate across the optode membrane and temperature (Bittig et al. 2014), and it can be calculated accurately for the SBE63 in a pumped flow (Bittig and Körtzinger 2017). In the temperature range of 2°–20°C, τ ranges from approximately 30 to 40 s. Bittig et al. (2014) presented a method to correct for sensor response time errors based on a single pole inverse filter method and demonstrated it can accurately reconstruct in situ O_2 profiles. However, this approach can amplify noise, particularly in stable parts of the water column such as the mixed layer. For example, during a mission in February 2020, the precision (1σ) in the well mixed surface layer increased from ±0.14 to ±0.40 μmol kg^{-1} when the correction was applied. While this level of noise may seem small, it could introduce errors into sensitive calculations such as for air–sea flux (Bushinsky et al. 2017) and net community production (Martz et al. 2008; Plant et al. 2016), thus it should be minimized if possible. It is important to note that the Bittig et al. (2014) correction on platforms with lower vertical resolution, such as profiling floats, does not seem to noticeably increase instrumental noise, even on continuous profiling mode floats that measure every 2 m.

Brought to you by NOAA Central Library | Unauthenticated | Downloaded 08/13/24 07:32 PM UTC

The amplified noise can be minimized by filtering the data prior to reconstruction (Gordon et al. 2020). The discretized form of the inverse-filter approach in Bittig et al. (2014) can be expressed as [by rearranging their Eq. (A3)]:

$$\frac{O_{2,in}(t)+O_{2,in}(t-1)}{2}=\frac{O_{2,opt}(t)+O_{2,opt}(t-1)}{2}+\tau\frac{\Delta O_{2,opt}}{\Delta t} \quad \text{and} \tag{2}$$

$$\frac{\Delta O_{2,opt}}{\Delta t}=\frac{O_{2,opt}(t)-O_{2,opt}(t-1)}{\Delta t}, \tag{3}$$

where $O_{2,in}$ refers to the "real" in situ O_2, $O_{2,opt}$ is the O_2 measured by the optode, t represents time points, and Δt is the difference in time between t and $t-1$. The $[O_{2,in}(t)+O_{2,in}(t-1)]/2$ is then interpolated back onto the original time stamp. It is assumed at $O_{2,in}=O_{2,opt}$ at $t=0$. Here, we applied a 7-point running mean filter on $\Delta O_{2,opt}/\Delta t$ prior to Eq. (3) in order to minimize instrumental noise from being amplified. This filter size was chosen because it was the lowest to achieve similar standard deviation in the mixed layer as the raw O_2 output. However, filtering the raw data has the downside of altering the structure of the vertical distribution of O_2 by reducing the peaks of finescale structures, as well as steepening the oxycline. Therefore, we only applied the running mean filter when $\Delta O_{2,opt}/\Delta t < 0.06\,\mu mol\,kg^{-1}\,s^{-1}$, or approximately $0.6\,\mu mol\,kg^{-1}\,m^{-1}$. In this region, this roughly represents ~40% of the water column, typically in the mixed layer or at depth. This threshold was chosen, because the mean standard deviation of uncorrected $O_{2,opt}$ in a well-mixed surface layer was ±0.14, and this threshold corresponds to $\sim 4\sigma$. This ensures that instrumental noise will get filtered, but environmental gradients that are significantly larger than instrumental noise will not get filtered, preserving real oxygen variability as much as possible.

c. *Empirical algorithms*

The accuracy of empirical algorithms to estimate pH and TA along the central CCS was assessed using hydrographic data from the West Coast Ocean Acidification (WCOA) 2016 cruise (Alin et al. 2017), and from the two MBARI-led Central California Coast pH, and Oxygen (C3PO) cruises in 2019. Cruise data spanned transects from Point Conception to Point Arena (Fig. 1). All cruises analyzed here utilized purified metacresol purple indicator dye (Liu et al. 2011). pH estimated using CANYON-B ($pH_{CANYON\text{-}B}$) is derived from pH calculated from TA and DIC (Bittig et al. 2018b). However, there is a known linear pH-dependent error between pH calculated from TA and DIC compared to direct measurements of pH using spectrophotometry, with a slope of approximately 0.04 (Carter et al. 2018; Fong and Dickson 2019; Takeshita et al. 2020). Therefore, a correction was made to $pH_{CANYON\text{-}B}$ based on Eq. (1) in Carter et al. (2018) so it is consistent with spectrophotometric pH measurements. $pH_{CANYON\text{-}B}$ showed slightly better agreement with the discrete samples compared to the multiple linear locally interpolated pH regression (LIPHR) model (Carter et al. 2018), thus it will be utilized hereafter. We utilized the default acidification setting for LIPHR, which may have contributed to the increased discrepancy. For example, modeling results suggest that the acidification rate in the CCS is higher than other parts of the ocean (Gruber et al. 2012). As density-specific acidification rates are not available in this region, we could not correct for this error.

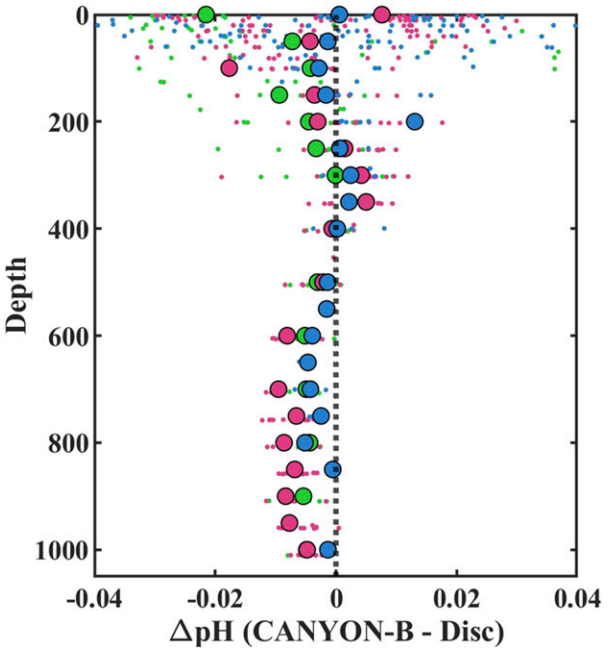

FIG. 3. Depth profile of the residual between CANYON-B and discrete samples of pH from the 2016 WCOA cruise (blue), C3PO May (pink), and C3PO July (green). Large filled circles represent 50 m binned averages.

On average, the bottle pH and estimated pH from CANYON-B agreed to better than ±0.01 below about 200 m (Fig. 3). All three cruises showed similar patterns with depth, where very close agreement (±0.005, 1σ) was observed between 350 and 550 m depth. Below 550 m the estimated pH was systematically lower than the measured pH by about 0.01. The difference between the algorithm and WCOA16 was smaller relative to C3PO, and this could reflect spatial differences in the two cruises, as C3PO had higher sample density throughout the study region. These comparisons suggest that estimated pH from depths between 350 and 550 m in the central to Northern California region are accurate to better than ±0.005, and thus can be utilized to assess pH sensor drift from gliders. The typical dive depth for our missions was 500 m, thus sensor drift was assessed at 450 m. TA estimated from locally interpolated alkalinity regression (LIAR), version 2 (LIARV2; Carter et al. 2018), and CANYON-B had similar performances, with a RMSE of ±6.4 and ±6.8 $\mu mol\,kg^{-1}$ ($n = 1138$), respectively. For simplicity, we used CANYON-B-estimated TA to derive other carbonate parameters.

d. *Validation of glider pH and O_2*

Discrete samples for pH, TA, and O_2 were collected alongside the glider using a shipboard rosette on 14 different occasions ($n = 168$ for pH and TA, $n = 105$ for O_2), spanning between April 2019 and December 2019. Casts were conducted at the time of recovery or in the middle of the mission.

Brought to you by NOAA Central Library | Unauthenticated | Downloaded 08/13/24 07:32 PM UTC

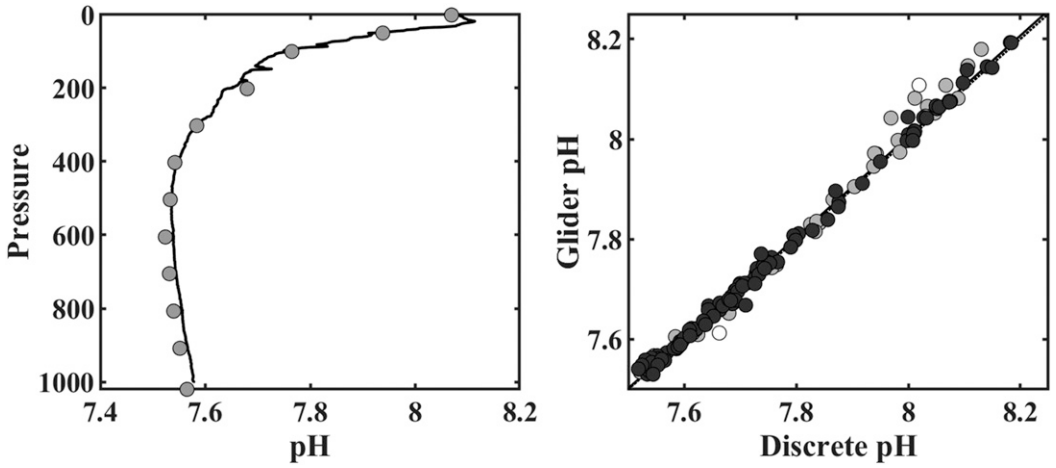

FIG. 4. (left) A typical profile of pH by the glider collected 29 May 2019 (36.5753°N, 122.598°W) (line) and discrete samples (circles). (right) Glider pH vs discrete pH ($n = 155$) over 14 casts. Light gray and white circles were not included in the comparison because they represent data where temperature discrepancies were >0.1°C and outliers (pH discrepancy > 0.05), respectively. Dark circles ($n = 112$) were used for the comparison. Solid line represents model II regression (slope = 1.005), and the dashed line is 1:1.

Comparison casts at the time of deployment were avoided, as a small, warm-up drift over several hours is often observed at the beginning of a deployment before stabilizing. All casts were conducted within 3 km and 12 h (average 2 km and 3.3 h) from the most recent glider surfacing. Samples were collected following standard protocols (Dickson 1996; Dickson et al. 2007). pH was measured spectrophotometrically (Clayton and Byrne 1993) using purified metacresol purple indicator dye (Liu et al. 2011) with an automated benchtop system based on the design in (Carter et al. 2013). Precision and accuracy are estimated to be ±0.0007 and ±0.003, respectively. TA was measured using a semiautomated titrator (Metrohm 855) using an open-cell, modified Gran titration (Dickson et al. 2003). Samples were run in triplicate with an average precision and accuracy of $\pm 2\,\mu\text{mol kg}^{-1}$. pH was converted to in situ conditions using CO2SYS (van Heuven et al. 2011). O_2 was measured via Winkler Titration (Carpenter 1965) with a photometric endpoint detection. KIO_3 standards were recrystallized 4 times to remove impurities (Emerson 1999), and the titrant was standardized gravimetrically (Martz et al. 2012). The precision and accuracy of the O_2 measurements are estimated to be ±0.5 and $\pm 1\,\mu\text{mol kg}^{-1}$, respectively. Comparisons between glider data and discrete samples were made on isopycnal surfaces, except for the surface samples where they were compared at equal depths.

3. Results and discussion

a. Assessment of pH sensor performance

Since April of 2019, the pH-Spray conducted 7 missions for a total of 161 glider days, and over 1600 dives to a maximum depth of 1000 m, including three transects to 250–300 km offshore of Monterey Bay in April–May 2019, July–August 2019, and February–March 2020; the transects followed California Cooperative Oceanic Fisheries Investigations (CalCOFI) line 67 (Fig. 1). The pH data presented utilized the same k_0 for all deployments, which was determined prior to the first deployment. A typical pH profile from the glider from 29 May (36.5753°N, 122.598°W) is shown in Fig. 4.

In general, good agreement was observed between discrete and glider pH, with a mean difference of 0.006 ± 0.021 (1σ, $n = 155$). However, it is important to be mindful that some of the discrepancy between glider measurements and discrete samples are driven by real spatiotemporal differences between the glider and bottle samples. To minimize such discrepancies, samples where the temperature difference was greater than 0.1°C (a proxy for different water masses), as well as two outliers were removed where the difference in pH was greater than 0.05, leaving 112 samples for comparison. After applying this criteria, the mean difference improved to −0.003 ± 0.011 (1σ), and we interpret this as the sensor accuracy. These discrete samples were taken over ~8 months, demonstrating consistent and accurate sensor behavior over multiple deployment and recovery cycles, which is an enabling result for routine glider operations.

For the first 9 months of deployments, glider pH agreed with deep reference pH to better than ±0.01, indicating minimal sensor drift (Fig. 5). Although there were small offsets in pH on the order of several milli-pH between deployments, pH was stable throughout each deployment. These small offsets were likely caused by either power cycling the ISFET circuitry, or the dehydration/hydration cycle of the reference electrode between deployments. However, two noticeable patterns emerged in the last deployment. First, the ΔpH ($pH_{spray} - pH_{CANYON\text{-}B}$) was different between dives to 550 m compared to those down to 1000 m, indicating the emergence of a pressure hysteresis in the sensor performance. The magnitude of this hysteresis was approximately 0.007. Some previous deployments showed hysteresis effects as well, but with smaller magnitudes (Fig. 5). It is not clear what caused this pressure hysteresis effect to appear, but small pressure

Brought to you by NOAA Central Library | Unauthenticated | Downloaded 08/13/24 07:32 PM UTC

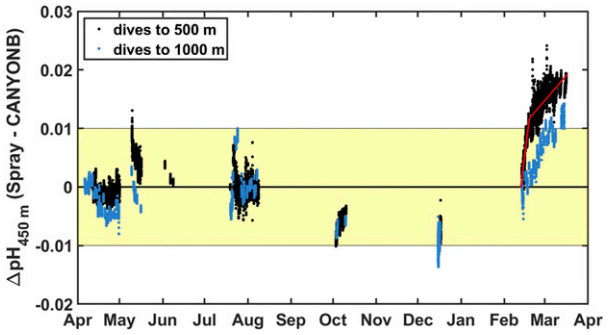

FIG. 5. A yearlong record (April 2019–April 2020) of the stability of glider pH at 450 m (reference depth) when the glider was outside of Monterey Bay, defined as west of 122.3°W. The difference between glider pH and reference pH from 500 and 1000 m dives are plotted in black and blue, respectively. Reference pH was calculated using CANYON-B (Bittig et al. 2018b). The yellow box represents ±0.01. Piecewise linear regression to correct for sensor drift for the final deployment is shown in the red line.

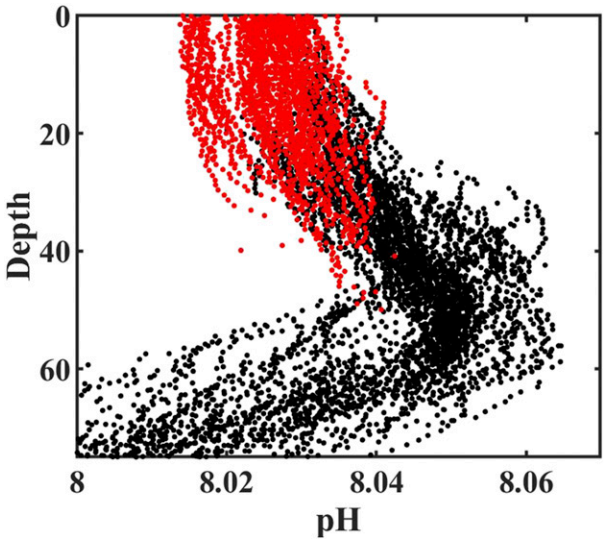

FIG. 6. pH profiles of the upper 75 m in July 2019 collected 250–300 km offshore of Monterey Bay. Red dots indicate measurements made in the mixed layer, defined with a temperature threshold of $\Delta T = 0.2$°C.

hysteresis effects have been observed in the laboratory (Johnson et al. 2016; Takeshita et al. 2017). Second, a noticeable positive drift in glider pH was observed during the last mission, where the sensor drifted for several weeks and then stabilized. The cause of this drift at this time is unknown but is correctable by adjusting the k_0 (constant term in the calibration coefficient) using a piecewise linear regression (two segments) so that the glider pH matches the algorithm pH (Fig. 5); this approach has been demonstrated to be effective for profiling floats (Johnson et al. 2016, 2017; Takeshita et al. 2018). Unfortunately, discrete samples were not collected alongside the glider for the last deployment, thus this correction could not be validated. Future efforts will focus on validating this drift correction approach. Furthermore, we hypothesize that the drift was caused by biofouling, and we plan to clean the pH sensor surface between deployments moving forwards.

Precision of the pH measurements were assessed by examining measurements in the mixed layer (Fig. 6). Assuming that the mixed layer is homogeneous in pH, as well as temperature, the precision of the instrument can be estimated as the variability (defined as 1σ) of pH in the mixed layer for each profile. We defined the mixed layer depth using a temperature threshold criterion of $\Delta T = 0.05°$, 0.1°, and 0.2°C, and the average mixed layer depth was 16, 20, and 23 m, respectively. Data from 250 to 300 km offshore in July 2019 were used (n = 71 profiles), as this region had deeper mixed layers relative to inshore, as well as has less dynamic coastal processes that induces natural variability such as eddies and upwelling. The median standard deviation of all pH profiles in the mixed layer was 0.0008 ± 0.0016 ($\Delta T = 0.05$°C), 0.0011 ± 0.0016 (ΔT = 0.1°C), and 0.0016 ± 0.0016 ($\Delta T = 0.2$°C). The near linear increase between ΔT and variability in pH in the mixed layer indicates that a larger temperature threshold incorporates real vertical pH differences. Therefore, we use the smallest temperature threshold of $\Delta T = 0.05$°C to estimate the mixed layer depth. However, we report the precision of the pH sensor as ±0.0016, calculated as double the observed variability in the mixed layer as an upper limit to account for instrumental variability. The precision of this instrument demonstrates its ability to accurately capture fine spatial and temporal differences in carbonate parameters.

Sensor response time was assessed on a mission conducted in December 2019 by collecting measurements on both the ascent and descent approximately 50 km offshore of MBARI, as the spatiotemporal variability at this site was lower than inside Monterey Bay. Five dives were conducted to 1000 m depth while holding station and were used for this analysis. We limit the analysis to these five dives as other dives in this mission were conducted during transit, thus, would introduce additional variability from spatial differences. However, comparisons between ascent and descent profiles have inherent uncertainties that make it difficult to make quantitative conclusions about response times. For example, internal waves can shoal or deepen isopycnal surfaces (and associated chemical properties) between the ascent and descent that lead to differences that are not related to sensor response time (Rudnick 2016). In addition, there are submesoscale variabilities on the order of kilometers (Nam et al. 2015) that will lead to differences in the two profiles due to different water mass properties. Finally, water must flow around the glider before it reaches the intake that is located on the topside, thus can lead to increased noise and a delayed response on the descent relative to the ascent (Davis et al. 2008). Given these uncertainties, we interpret these profile comparisons as a qualitative assessment of sensor response and acknowledge that controlled laboratory studies are required to fully characterize sensor response errors (Bittig et al. 2014).

In general, excellent reproducibility between up and down casts was observed below 500 m where water properties were stable and vertical gradients were small (Fig. 7). The mean discrepancy for pH was −0.0001 ± 0.0006 (1σ; Table 1). However, since this

Brought to you by NOAA Central Library | Unauthenticated | Downloaded 08/13/24 07:32 PM UTC

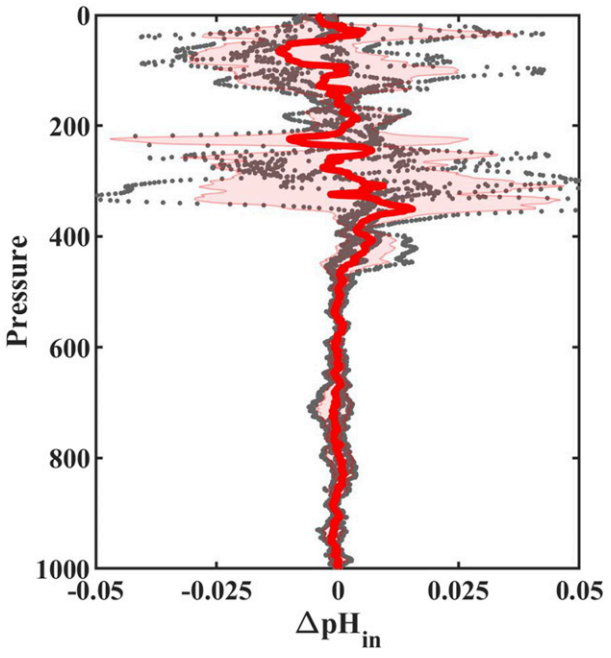

FIG. 7. Residuals (descent minus ascent) for pH from five dives to 1000 m outside Monterey Bay. Gray dots represent 1 m binned data,the red line represents the mean, and shaded error bars represent $\pm 1\sigma$.

part of the water column is relatively stable, it does not provide much insight into sensor response times. On the other hand, it does demonstrate that pressure hysteresis effects were minimal during this mission. The discrepancy increased above 500 m for all four parameters, and the mean discrepancy for pH was 0.0012 ± 0.0053 (1σ). Large discrepancies in pH and O_2 typically coincided with discrepancies in temperature and salinity that could be as large as 0.5°C and 0.1 salinity, respectively, suggesting the glider was measuring different water masses at times. Nonetheless, on average there was good agreement throughout the water column with no systematic patterns for pH. In particular, there was no pronounced positive bias for pH in the upper 200 m where the vertical gradient is the greatest. If sensor response time were a substantial source of error, we would expect a positive trend in this part of the water column. Finally, the fact that the discrete samples agreed with sensor pH throughout the water column with no correction (Fig. 4) provides further support that sensor response time is not a major issue for this system. Given this line of reasoning, we believe that sensor response errors in pH is minimal, but further studies are required to verify this.

Each derived variable had distinct patterns in the propagated overall uncertainty (Fig. 8). For example, pCO_2 had a relatively constant percent uncertainty (2.1%–2.5%) between 300 and 1400 μatm, which translates to an absolute uncertainty of ± 6 to ± 35 μatm over this range. Our uncertainty estimate at 400 μatm (± 9 μatm) is in good agreement with a bottom-up uncertainty analysis for profiling float pH, where they estimated ± 11 μatm (Williams et al. 2017). The hooking feature around 1200–1400 μatm is due to the fact that there is a pCO_2 maximum around 600 m, whereas TA continues to steadily

TABLE 1. Mean $\pm 1\sigma$ of the residual (descent minus ascent) of temperature (°C), salinity, O_2 (μmol kg^{-1}), and pH_{in} in the upper 500 m and the lower 500 m.

	1–500 m	500–1000 m
Temperature	0.038 ± 0.107	-0.011 ± 0.018
Salinity	0.004 ± 0.010	0.004 ± 0.003
O_2	3.13 ± 2.34	0.02 ± 0.20
pH_{in}	0.0012 ± 0.0053	-0.0001 ± 0.0006

increase from ~2230 to 2370 μmol kg^{-1} from the surface to depth, thus the propagated uncertainty is slightly different above and below the pCO_2 maximum. However, the changing absolute uncertainty could have implications for air–sea flux studies in the coastal ocean. For example, we observed surface pCO_2 between 300 and 800 μatm across all of our deployments. The percentage uncertainty results in a pCO_2 error that is dependent on the surface condition, thus ranges from ± 6 to ± 17 μatm, and its implications for the calculated air–sea flux should be considered accordingly. On the other hand, the uncertainty for Ω_{Ar} decreased as CO_2 levels increased and was always better than 2%. Near atmospheric conditions, Ω_{Ar} could be estimated to ± 0.05, whereas the uncertainty decreased to ± 0.02 near saturation ($\Omega_{Ar} = 1$). It is worth noting that this is approaching the "climate quality" measurement standards of $\pm 1\%$, set by the Global Ocean Acidification Observing Network (Newton et al. 2014). Finally, the uncertainty for derived DIC was relatively constant across all conditions and ranged from 6.8 to 7.6 μmol kg^{-1}.

Properly protecting the ISFET from solar irradiance is critical, as it can cause large biases in the measured pH near the surface. Our earlier iteration of the flow cell during the development phase prior to data presented here was 3D printed with a semitransparent urethane resin, leading to erroneously high readings due to light contamination near the surface (Fig. 9). Light sensitivity for ISFETs have been previously reported (Hemming et al. 2017), although their pH bias under solar irradiation was negative. Based on our experience, the light sensitivity is specific for each Honeywell ISFET, causes a positive pH bias, and can be as large as >0.02 under ambient room light conditions and >0.35 pH in sunlight for this ISFET. This light contamination problem was significantly reduced, but still noticeable when the flow cell was machined out of black Delrin, and the tubing connecting the inlet and outlet were switched to black Tygon. We discovered that the sunlight contamination originated from the white-Delrin flow cap for the SBE5SM pump, which was connected to the DSD flow cell by ~2 in. (~5 cm) of opaque tubing. No light contamination was observed when the flow cap for the pump was switched to black Delrin. This demonstrates how sensitive the DSD is to potential light contamination, and that it is imperative to pay close attention to any potential light contamination pathways and to verify this with monitoring the appropriate diagnostics to obtain accurate pH measurements. In particular, the ISFET base current increases when exposed to light.

Biofouling is always a challenge for successful operation of autonomous platforms and sensors in the ocean. Visual inspection

Brought to you by NOAA Central Library | Unauthenticated | Downloaded 08/13/24 07:32 PM UTC

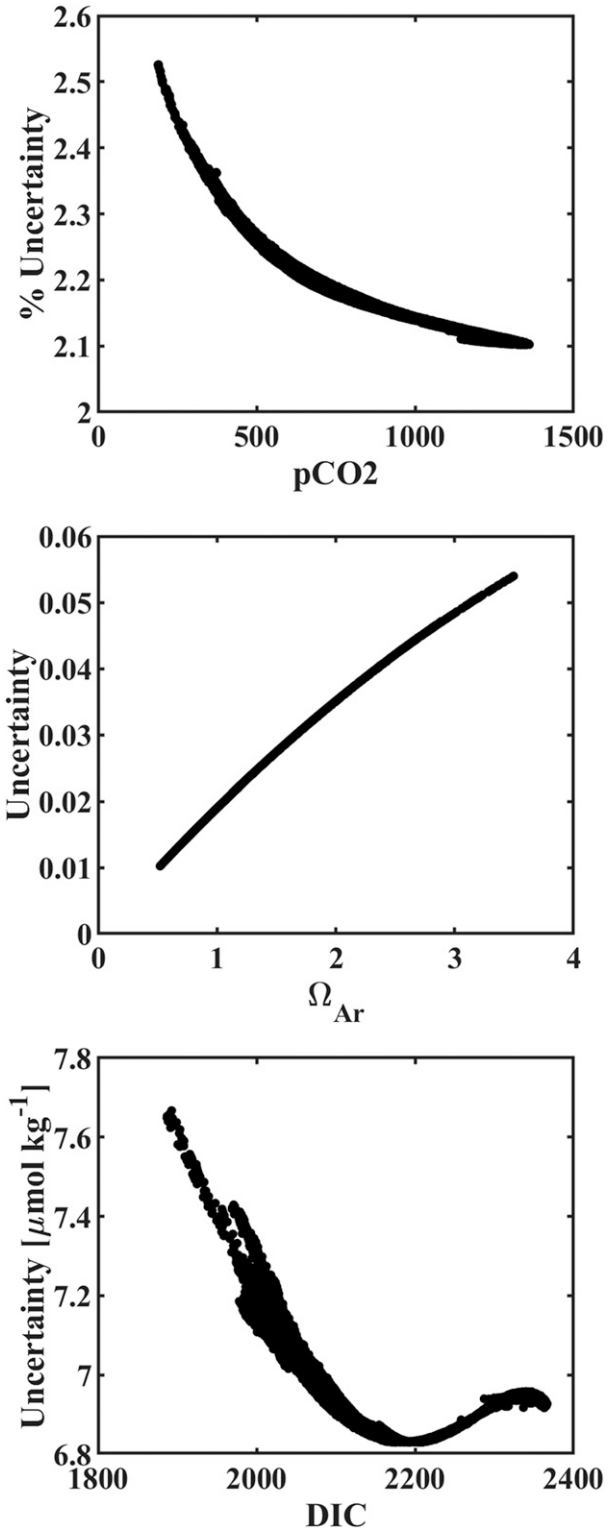

FIG. 8. Propagated uncertainty for (top) pCO_2 (expressed as a percentage),(middle) Ω_{Ar}, and (bottom) DIC as a function of their respective parameters from a month long mission in April 2019. Uncertainties were calculated using Monte Carlo simulations (100 runs), assuming an uncertainty in pH, TA, and nutrients of ±0.01, ±6.8 μmol kg^{-1}, and ±20%, respectively.

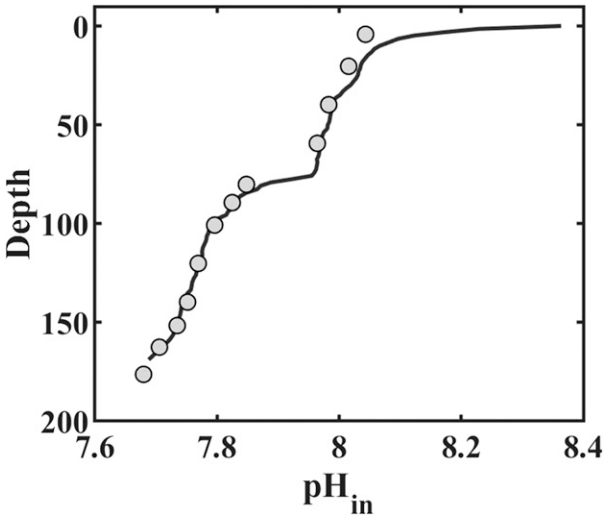

FIG. 9. Example of a light-contaminated pH profile in Monterey Bay. pH from the glider and discrete samples is represented by the black line and gray dots, respectively. A clear, positive bias in glider pH is observed in the upper 40 m due to light contamination.

of the pH sensor after deployments, as well as the stability of deep pH values (Fig. 5) indicate that biofouling was not a major issue for our glider operations. This was true even through month long summertime missions where large phytoplankton blooms were present where surface O_2 saturation was as high as 140%. The sensors were not cleaned between deployments, except for a brief deionized water rinse after each deployment. We believe that having a pumped flow stream with antifouling plugs in the CTD is critical to effectively combat biofouling (Davis et al. 2008). Furthermore, only collecting data on the ascent allows for the antifouling compounds to permeate in the flow stream, further increasing their effectiveness. However, the impact of biofouling is likely to be dependent on deployment location, season, and glider mission parameters. For example, Saba et al. (2019) reported biofouling as a major limitation for pH glider missions lasting only several weeks during summertime over the continental shelf on the East Coast of the United States. Likely, the warmer water temperatures and shallow dive depths (tens of meters) exacerbated the effects of biofouling, as their glider mostly resided in the euphotic zone. The shallowest dives for our glider missions were 200 m, which was approximately the depth of their deepest dive. Thus, diving to depths that are significantly deeper than the euphotic zone seems to be important to minimize biofouling. If conducting deeper dives is not possible due to shallow waters, additional antibiofouling measures are likely necessary. Tubing could be made of copper or turning on the pump only on the ascent could help antifouling plugs in the CTDs to permeate the flow cell.

One of the benefits for glider operations is that sensors can be easily replaced when sensor performance starts to degrade. Furthermore, the failed sensor can be used to diagnose failure mechanisms, which allow for refinement and improvement toward a more robust sensor design. Currently DSDs are primarily deployed on profiling floats, which are rarely recovered,

Brought to you by NOAA Central Library | Unauthenticated | Downloaded 08/13/24 07:32 PM UTC

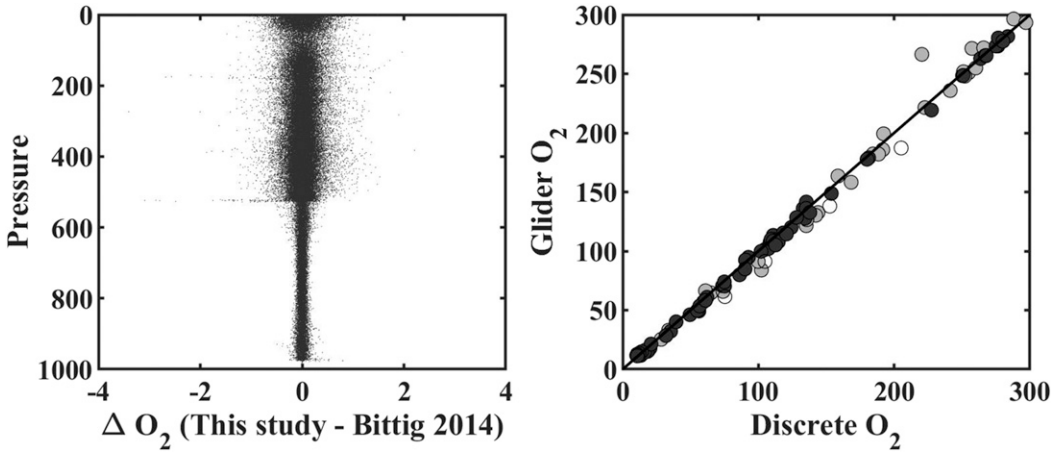

FIG. 10. (left) Difference in time-corrected O_2 between this study and that of Bittig et al. (2014). (right) Glider O_2 vs bottle O_2 from 14 hydrocasts ranging from 0 to 1000 m over 9 months. Glider O_2 values were corrected for sensor response time. Comparisons were made only using the dark circles ($n = 68$). Light gray circles represent data where the difference in temperature was >0.1°C, and white circles represent four outliers. The solid line is 1:1.

thus sensor failures cannot be diagnosed. Furthermore, there can be lags of up to a year between sensor design modification and float deployments, which hinders sensor refinement efforts. Operating and testing refined designs on gliders can shorten the time for this feedback loop, and thus lead to more efficient sensor improvements.

b. O_2

The sensor lag correction method proposed in this study produced very similar results as the method described in Bittig et al. (2014) to correct for sensor response (Fig. 10). Some 97.8% of the data from both methods were within 0.5 μmol kg^{-1}, 99.8% within 1 μmol kg^{-1}, and 99.99% within 2 μmol kg^{-1}. The differences between the two methods occur in low O_2 gradient regions, where sensor noise was likely amplified using Bittig et al. 2014. For example, the average precision (1 σ) in the mixed layer from a mission in February 2020 was ±0.14, ±0.16, and ±0.40 μmol kg^{-1} ($n = 64$ profiles) for raw $O_{2,opt}$, O_2 corrected from this study, and O_2 corrected using Bittig et al. (2018), respectively. This demonstrates that the selective filtering method proposed here prevented noise from getting amplified into the corrected data. It is likely that the correction for sensor time errors is more accurate for pumped optodes such as the SBE63 rather than optodes that are passively flushed through the vertical movement of the platform, as the boundary layer thickness can be more accurately parameterized and their response time is faster (Bittig and Körtzinger 2017). The downside of a pumped optode is that it cannot be air calibrated in situ.

Consistent gain correction factors were obtained over 8 months and the mean G was 1.033 ± 0.007 (1σ, $n = 6$). No systematic trend over time was detected, thus the mean G was used to correct O_2 data from all missions. The comparison between glider and bottle O_2 are shown in Fig. 10. Similar to pH, comparisons were only made when the temperature was consistent to ±0.1°C, and four outliers were removed, leaving 62 comparisons. After applying the sensor time response correction, the mean difference between the glider and discrete O_2 was −2.1 ± 2.9 (1σ) μmol kg^{-1}, which is lower than 1% error relative to typical surface O_2 in this region. The slope of the model II regression was 0.996 ± 0.004. The slight low bias of the correction could be due to errors in the atmospheric pressure or humidity used for the air calibration. In the future, we plan to utilize a barometer with higher accuracy, as well as pumping prehumidified air through the flow cell to ensure 100% humidity during calibration. If the response time correction was not applied, the mean difference was −3.0 ± 3.7 μmol kg^{-1}, and the distribution was skewed toward negative biases where errors with magnitude greater than 10 μmol kg^{-1} were observed during high oxygen gradients. These comparisons demonstrate that the calibration protocol and sensor response time correction presented here are capable of achieving accurate O_2 throughout the water column.

The gain for the O_2 sensor could have been calculated by directly measuring O_2 using Winkler titrations (Carpenter 1965) alongside the sensor pre and post deployment. While this would provide the most accurate results, it would require detaching the O_2 sensor frequently, leading to potential failure mechanisms. Furthermore, the research groups would need to maintain equipment and expertise to conduct accurate Winkler titrations, which is demanding, especially if measurements are not made routinely. Finally, it is not always possible to conduct Winkler calibrations directly prior to deployments, for example, for remote deployments. Thus, our objective was to develop a simple calibration protocol that can be implemented in any situation without specialized equipment. While this approach cannot accurately assess any potential sensor drift that occurred during the deployment, it provides a simple and robust calibration protocol that can be easily implemented by any research group. This approach can also be adopted to any platform including shipboard underway measurements, moorings, wave gliders, and profiling floats.

c. *Upwelling and submesoscale variability near Monterey Bay*

Glider observations over a year revealed highly dynamic, submesoscale variability (spatial scales <10 km) of pH in the

Brought to you by NOAA Central Library | Unauthenticated | Downloaded 08/13/24 07:32 PM UTC

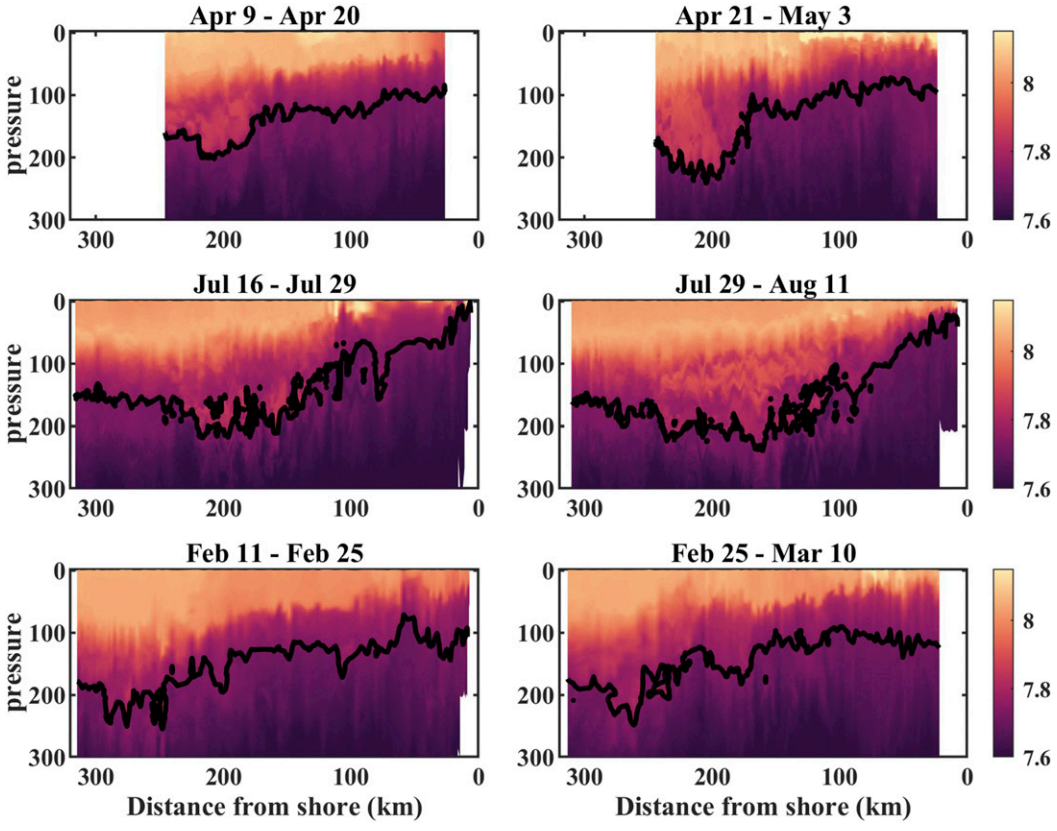

FIG. 11. pH contour plots of the upper 300 m along a transect from Monterey Bay to 300 km offshore (Fig. 1), using the cmocean color map (Thyng et al. 2016). The columns represent (left) outgoing and (right) incoming transects from each mission. The black line represents the saturation horizon for Ω_{Ar}.

upper 300 m along a transect to 250–300 km offshore from Monterey Bay (Fig. 11). Six transects were collected over a year (April–May 2019, July–August 2019, and February–March 2020), including two during an upwelling event in July–August 2019. During such events, isopycnal surfaces can shoal by up to 100 m, bringing deep, low-pH waters to the surface. In fact, during one transect, corrosive waters with respect to aragonite ($\Omega = 0.995$, pH = 7.718) was observed in the top 5 m inside Monterey Bay. Furthermore, finescale submesoscale features were more prominent between 100 and 200 m depth during these transects, which correlated with spice. This suggests that these features were driven by different proportion of water masses in the California Undercurrent (Thomson and Krassovski 2010; Nam et al. 2015). Capturing and understanding the variability of these water masses is important, as they serve as the source water for upwelling. Autonomous glider observations are well suited to observe these dynamics on seasonal (Nam et al. 2015) to interannual (Bograd et al. 2015) time scales. Finally, the submesoscale features in the midwater were highly dynamic, and changed on time scales of days to weeks. For example, the saturation horizon deepened by 30–40 m approximately 200 km offshore within a couple of days in April 2019, as seen by comparing the outgoing and incoming transects from that mission (Fig. 11). Changes in finescale variability is observed from other missions as well. This highlights the importance of sustained, high-spatiotemporal resolution observations obtainable by underwater gliders in highly dynamic coastal systems such as the CCS.

4. Conclusions

In this paper, we presented a Deep-Sea-DuraFET pH-sensor payload for Spray gliders, which exhibited excellent accuracy (±0.011) and precision (±0.0016) over multiple missions spanning about one year. The sensor was stable to better than ± 0.01 between missions, except during the last mission when a drift of 0.015 was observed. However, this drift could be corrected based on a deep reference pH field at 450 m computed from existing global empirical algorithms. Protocols for achieving accurate O_2 measurements that are necessary for these algorithms were also developed. These extremely encouraging results demonstrate the strong potential for this new technology to enable sustained, autonomous high-resolution pH measurements in the coastal ocean, where such observations are critically lacking.

There is currently a network of Spray gliders operating in the CCS [California Underwater Glider Network (CUGN)], consisting of three lines that have been continuously occupied since 2007, including CalCOFI line 67 described in this paper, and two new lines that were added in 2019 (Rudnick et al. 2017). If the

Brought to you by NOAA Central Library | Unauthenticated | Downloaded 08/13/24 07:32 PM UTC

CUGN gliders were equipped with pH sensors, it could lead to sustained, high-resolution monitoring of coastal acidification dynamics in the CCS. The DSD pH sensor would have minimal impact on the power budget. The Sprays in the CUGN dive to depths of 500 m, enabling a robust sensor-drift correction at 450 m, which is a critical component for obtaining accurate measurements from an observational network. However, the current CUGN Spray gliders are at payload capacity, thus adding the DSD pH sensor would require removing a sensor or adding a second glider on each line. Another possibility is to transition to a glider with higher payload capabilities, like the Spray 2 glider currently under development. The prospect of enhancing the CUGN with pH observations is particularly exciting, because biological and ecological impacts of acidification dynamics can be studied. For example, the sustained glider pH observations could provide insights into exposure history of pteropods *Limacina helicina* to high CO_2 conditions to better assess the impacts of ocean acidification on this important organism (Bednaršek et al. 2017). The collocation of glider observations with CalCOFI is in direct alignment with goals and objectives outlined in the GOA-ON requirements (Newton et al. 2014).

Looking forward, the modular design of this DSD-pH payload makes it relatively straightforward to integrate onto other glider types such as Seagliders (Eriksen et al. 2001), increasing its potential for routine use by the wider oceanographic community. There is a growing number of sustained glider monitoring programs worldwide (Testor et al. 2019), thus providing an opportunity to significantly enhance our global observational capacity for coastal acidification using this new technology. Further refinement in sensor design and reliability, as well as close coordination and efficient knowledge transfer through shared standard protocols, will be critical to achieve this grand vision.

Acknowledgments. This work was funded by the David and Lucile Packard Foundation. We thank the Naval Postgraduate School for their support for Spray glider maintenance. We thank the Instrument Development Group at Scripps Institution of Oceanography for the use of their servers for piloting and data transmission. Peter Walz assisted with sensor calibration and diagnosis. We are grateful for Jared Figurski, Chris Wahl, Charmaine Yung, and Erich Reinicker for their aid in deployment and recovery of the Spray glider, as well as the collection of discrete samples. We thank the science party, Emily Bockmon, Sara Gray, Kate Hewett, Heidi Hirsh, Addie Norgaard, and Maddie Verburg, and the captain and crew of the R/V *Western Flyer* during the C3PO cruises. We thank NOAA's Ocean Acidification Program and the Pacific Marine Environmental Laboratory for supporting the WCOA 2016 cruise. DLR thanks NOAA Ocean Observing and Monitoring Division (NA15OAR4320071) and Integrated Ocean Observing System (NA16NOS012022) for their support.

Data availability statement. Spray glider data are publicly available through CeNCOOS, or via the GliderVIZ portal (www.mbari.org/gliderviz). Data from the C3PO cruises are currently in the process of being uploaded to NCEI.

REFERENCES

Alin, S. R., R. A. Feely, B. Hales, R. H. Byrne, W. Cochlan, X. Liu, and D. Greeley, 2017: Dissolved inorganic carbon, total alkalinity, pH on total scale, and other variables collected from profile and discrete sample observations using CTD, Niskin bottle, and other instruments from NOAA Ship *Ronald H. Brown* in the U.S. West Coast California Current System from 2016-05-08 to 2016-06-06 (NCEI Accession 0169412), Stations 30–62. NOAA/National Centers for Environmental Information, accessed 20 July 2019, https://doi.org/10.7289/v5v40shg.

Barton, A., B. Hales, G. G. Waldbusser, C. Langdon, and R. A. Feely, 2012: The Pacific oyster, *Crassostrea gigas*, shows negative correlation to naturally elevated carbon dioxide levels: Implications for near-term ocean acidification effects. *Limnol. Oceanogr.*, **57**, 698–710, https://doi.org/10.4319/lo.2012.57.3.0698.

——, and Coauthors, 2015: Impacts of coastal acidification on the Pacific Northwest shellfish industry and adaptation strategies implemented in response. *Oceanography*, **25**, 146–159, https://doi.org/10.5670/oceanog.2015.38.

Bednaršek, N., R. A. Feely, J. C. P. Reum, B. Peterson, J. Menkel, S. R. Alin, and B. Hales, 2014: *Limacina helicina* shell dissolution as an indicator of declining habitat suitability owing to ocean acidification in the California Current ecosystem. *Proc. Biol. Sci.*, **281**, 20140123, https://doi.org/10.1098/rspb.2014.0123.

——, and Coauthors, 2017: Exposure history determines pteropod vulnerability to ocean acidification along the US West Coast. *Sci. Rep.*, **7**, 4526, https://doi.org/10.1038/s41598-017-03934-z.

Bittig, H. C., and A. Körtzinger, 2015: Tackling oxygen optode drift: Near-surface and in-air oxygen optode measurements on a float provide an accurate in situ reference. *J. Atmos. Oceanic Technol.*, **32**, 1536–1543, https://doi.org/10.1175/JTECH-D-14-00162.1.

——, and ——, 2017: Technical note: Update on response times, in-air measurements, and in situ drift for oxygen optodes on profiling platforms. *Ocean Sci.*, **13** (1), 1–11, https://doi.org/10.5194/os-13-1-2017.

——, B. Fiedler, R. Scholz, G. Krahmann, and A. Körtzinger, 2014: Time response of oxygen optodes on profiling platforms and its dependence on flow speed and temperature. *Limnol. Oceanogr. Methods*, **12**, 617–636, https://doi.org/10.4319/lom.2014.12.617.

——, and Coauthors, 2018a: Oxygen optode sensors: Principle, characterization, calibration, and application in the ocean. *Front. Mar. Sci.*, **4**, 1–25, https://doi.org/10.3389/fmars.2017.00429.

——, T. Steinhoff, H. Claustre, B. Fiedler, N. L. Williams, R. Sauzède, A. Körtzinger, and J.-P. Gattuso, 2018b: An alternative to static climatologies: Robust estimation of open ocean CO_2 variables and nutrient concentrations from T, S, and O_2 data using Bayesian neural networks. *Front. Mar. Sci.*, **5**, 328, https://doi.org/10.3389/fmars.2018.00328.

Bograd, S. J., and Coauthors, 2015: Changes in source waters to the Southern California Bight. *Deep-Sea Res. II*, **112**, 42–52, https://doi.org/10.1016/j.dsr2.2014.04.009.

Bresnahan, P. J., T. R. Martz, Y. Takeshita, K. S. Johnson, and M. LaShomb, 2014: Best practices for autonomous measurement of seawater pH with the Honeywell Durafet. *Methods Oceanogr.*, **9**, 44–60, https://doi.org/10.1016/j.mio.2014.08.003.

Briggs, N., M. J. Perry, I. Cetinić, C. Lee, E. D'Asaro, A. M. Gray, and E. Rehm, 2011: High-resolution observations of aggregate flux during a sub-polar North Atlantic spring bloom. *Deep-Sea Res. I*, **58**, 1031–1039, https://doi.org/10.1016/j.dsr.2011.07.007.

Busch, D. S., and P. McElhany, 2016: Estimates of the direct effect of seawater pH on the survival rate of species groups in the California Current ecosystem. *PLOS ONE*, **11**, e0160669, https://doi.org/10.1371/journal.pone.0160669.

Brought to you by NOAA Central Library | Unauthenticated | Downloaded 08/13/24 07:32 PM UTC

Bushinsky, S. M., and S. Emerson, 2013: A method for in-situ calibration of Aanderaa oxygen sensors on surface moorings. *Mar. Chem.*, **155**, 22–28, https://doi.org/10.1016/j.marchem.2013.05.001.

——, ——, S. C. Riser, and D. D. Swift, 2016: Accurate oxygen measurements on modified Argo floats using in situ air calibrations. *Limnol. Oceanogr. Methods*, **14**, 491–505, https://doi.org/10.1002/lom3.10107.

——, A. R. Gray, K. S. Johnson, and J. L. Sarmiento, 2017: Oxygen in the Southern Ocean from Argo floats: Determination of processes driving air-sea fluxes. *J. Geophys. Res. Oceans*, **122**, 8661–8682, https://doi.org/10.1002/2017JC012923.

——, and Coauthors, 2019: Reassessing Southern Ocean air-sea CO_2 flux estimates with the addition of biogeochemical float observations. *Global Biogeochem. Cycles*, **33**, 1370, https://doi.org/10.1029/2019GB006176.

Carpenter, J. H., 1965: The Chesapeake Bay Institute technique for the Winkler dissolved oxygen method. *Limnol. Oceanogr.*, **10**, 141–143, https://doi.org/10.4319/lo.1965.10.1.0141.

Carter, B. R., J. A. Radich, H. L. Doyle, and A. G. Dickson, 2013: An automated system for spectrophotometric seawater pH measurements. *Limnol. Oceanogr. Methods*, **11**, 16–27, https://doi.org/10.4319/lom.2013.11.16.

——, R. A. Feely, N. L. Williams, A. G. Dickson, M. B. Fong, and Y. Takeshita, 2018: Updated methods for global locally interpolated estimation of alkalinity, pH, and nitrate. *Limnol. Oceanogr. Methods*, **16**, 119–131, https://doi.org/10.1002/lom3.10232.

Chan, F., J. A. Barth, J. Lubchenco, A. Kirincich, H. Weeks, W. T. Peterson, and B. A. Menge, 2008: Emergence of anoxia in the California Current large marine ecosystem. *Science*, **319**, 920, https://doi.org/10.1126/science.1149016.

Chavez, F. P., and M. Messié, 2009: A comparison of eastern boundary upwelling ecosystems. *Prog. Oceanogr.*, **83**, 80–96, https://doi.org/10.1016/j.pocean.2009.07.032.

——, and Coauthors, 2017: Climate variability and change: Response of a coastal ocean ecosystem. *Oceanography*, **30**, 128–145, https://doi.org/10.5670/oceanog.2017.429.

Clayton, T. D., and R. H. Byrne, 1993: Spectrophotometric seawater pH measurements: Total hydrogen ion concentration scale calibration of *m*-cresol purple and at-sea results. *Deep-Sea Res. I*, **40**, 2115–2129, https://doi.org/10.1016/0967-0637(93)90048-8.

D'Asaro, E., and C. McNeil, 2013: Calibration and stability of oxygen sensors on autonomous floats. *J. Atmos. Oceanic Technol.*, **30**, 1896–1906, https://doi.org/10.1175/JTECH-D-12-00222.1.

Davis, R. E., M. D. Ohman, D. L. Rudnick, J. T. Sherman, and B. Hodges, 2008: Glider surveillance of physics and biology in the Southern California Current System. *Limnol. Oceanogr.*, **53**, 2151–2168, https://doi.org/10.4319/lo.2008.53.5_part_2.2151.

Dickson, A. G., 1996: Determination of dissolved oxygen in sea water by Winkler titration. Standard Operating Procedure, World Hydrography Program, 13 pp., https://cchdo.github.io/hdo-assets/documentation/manuals/pdf/91_1/dickson2.pdf.

——, J. D. Afghan, and G. C. Anderson, 2003: Reference materials for oceanic CO_2 analysis: A method for the certification of total alkalinity. *Mar. Chem.*, **80**, 185–197, https://doi.org/10.1016/S0304-4203(02)00133-0.

——, C. L. Sabine, and J. R. Christian, Eds., 2007: Guide to best practices for ocean CO2 measurements. PICES Special Publ. 3, 191 pp., https://www.ncei.noaa.gov/access/ocean-carbon-data-system/oceans/Handbook_2007/Guide_all_in_one.pdf.

Dupont, S., E. Hall, P. Calosi, and B. Lundve, 2014: First evidence of altered sensory quality in a shellfish exposed to decreased pH relevant to ocean acidification. *J. Shellfish Res.*, **33**, 857–861, https://doi.org/10.2983/035.033.0320.

Emerson, S. R., 1999: Accurate measurement of O2, N2, and Ar gases in water and the solubility of N2. *Mar. Chem.*, **64**, 337–347, https://doi.org/10.1016/S0304-4203(98)00090-5.

Eriksen, C. C., T. J. Osse, R. D. Light, T. Wen, T. W. Lehman, P. L. Sabin, J. W. Ballard, and A. M. Chiodi, 2001: Seaglider: A long-range autonomous underwater vehicle for oceanographic research. *IEEE J. Oceanic Eng.*, **26**, 424–436, https://doi.org/10.1109/48.972073.

Evans, W., J. T. Mathis, P. Winsor, H. Statscewich, and T. E. Whitledge, 2013: A regression modeling approach for studying carbonate system variability in the northern Gulf of Alaska. *J. Geophys. Res. Oceans*, **118**, 476–489, https://doi.org/10.1029/2012JC008246.

Fong, M. B., and A. G. Dickson, 2019: Insights from GO-SHIP hydrography data into the thermodynamic consistency of CO_2 system measurements in seawater. *Mar. Chem.*, **211**, 52–63, https://doi.org/10.1016/j.marchem.2019.03.006.

Gordon, C., K. Fennel, C. Richards, L. K. Shay, and J. K. Brewster, 2020: Can ocean community production and respiration be determined by measuring high-frequency oxygen profiles from autonomous floats? *Biogeosciences*, **17**, 4119–4134, https://doi.org/10.5194/bg-17-4119-2020.

Gray, A. R., and Coauthors, 2018: Autonomous biogeochemical floats detect significant carbon dioxide outgassing in the high-latitude Southern Ocean. *Geophys. Res. Lett.*, **45**, 9049–9057, https://doi.org/10.1029/2018GL078013.

Gruber, N., C. Hauri, Z. Lachkar, D. Loher, T. L. Frölicher, and G.-K. Plattner, 2012: Rapid progression of ocean acidification in the California Current System. *Science*, **337**, 220–223, https://doi.org/10.1126/science.1216773.

Hauri, C., N. Gruber, G.-K. Plattner, S. Alin, R. Feely, B. Hales, and P. Wheeler, 2009: Ocean acidification in the California Current System. *Oceanography*, **22**, 60–71, https://doi.org/10.5670/oceanog.2009.97.

Hemming, M. P., and Coauthors, 2017: Measuring pH variability using an experimental sensor on an underwater glider. *Ocean Sci.*, **13**, 427–442, https://doi.org/10.5194/os-13-427-2017.

Jacox, M. G., E. L. Hazen, K. D. Zaba, D. L. Rudnick, C. A. Edwards, A. M. Moore, and S. J. Bograd, 2016: Impacts of the 2015–2016 El Niño on the California Current System: Early assessment and comparison to past events. *Geophys. Res. Lett.*, **43**, 7072–7080, https://doi.org/10.1002/2016GL069716.

Johnson, K. S., J. N. Plant, S. C. Riser, and D. Gilbert, 2015: Air oxygen calibration of oxygen optodes on a profiling float array. *J. Atmos. Oceanic Technol.*, **32**, 2160–2172, https://doi.org/10.1175/JTECH-D-15-0101.1.

——, H. W. Jannasch, L. J. Coletti, V. A. Elrod, T. R. Martz, Y. Takeshita, R. J. Carlson, and J. J. Connery, 2016: Deep-Sea DuraFET: A pressure tolerant pH sensor designed for global sensor networks. *Anal. Chem.*, 5b04653, https://doi.org/10.1021/acs.analchem.5b04653.

——, and Coauthors, 2017: Biogeochemical sensor performance in the SOCCOM profiling float array. *J. Geophys. Res. Oceans*, **122**, 6416–6436, https://doi.org/10.1002/2017JC012838.

——, J. N. Plant, and T. L. Maurer, 2018: Processing BGC-Argo pH data at the DAC level. Argo Data Management, 34 pp., https://doi.org/10.13155/57195.

Liu, X., M. C. Patsavas, and R. H. Byrne, 2011: Purification and characterization of meta-cresol purple for spectrophotometric seawater pH measurements. *Environ. Sci. Technol.*, **45**, 4862–4868, https://doi.org/10.1021/es200665d.

Lueker, T. J., A. G. Dickson, and C. D. Keeling, 2000: Ocean pCO_2 calculated from dissolved inorganic carbon, alkalinity,

Brought to you by NOAA Central Library | Unauthenticated | Downloaded 08/13/24 07:32 PM UTC

and equations for K_1 and K_2: Validation based on laboratory measurements of CO_2 in gas and seawater at equilibrium. *Mar. Chem.*, **70**, 105–119, https://doi.org/10.1016/S0304-4203(00)00022-0.

Martin, J. P., C. M. Lee, C. C. Eriksen, C. Ladd, and N. B. Kachel, 2009: Glider observations of kinematics in a Gulf of Alaska eddy. *J. Geophys. Res.*, **114**, C12021, https://doi.org/10.1029/2008JC005231.

Martz, T. R., K. S. Johnson, and S. C. Riser, 2008: Ocean metabolism observed with oxygen sensors on profiling floats in the South Pacific. *Limnol. Oceanogr.*, **53**, 2094–2111, https://doi.org/10.4319/lo.2008.53.5_part_2.2094.

——, J. G. Connery, and K. S. Johnson, 2010: Testing the Honeywell Durafet® for seawater pH applications. *Limnol. Oceanogr. Methods*, **8**, 172–184, https://doi.org/10.4319/lom.2010.8.172.

——, Y. Takeshita, R. Rolph, and P. Bresnahan, 2012: Tracer monitored titrations: Measurement of dissolved oxygen. *Anal. Chem.*, **84**, 290–296, https://doi.org/10.1021/ac202537f.

Mattern, J. P., H. Song, C. A. Edwards, A. M. Moore, and J. Fiechter, 2017: Data assimilation of physical and chlorophyll *a* observations in the California Current System using two biogeochemical models. *Ocean Modell.*, **109**, 55–71, https://doi.org/10.1016/j.ocemod.2016.12.002.

McLaughlin, K., and Coauthors, 2015: Core principles of the California Current acidification network: Linking chemistry, physics, and ecological effects. *Oceanography*, **25**, 160–169, https://doi.org/10.5670/oceanog.2015.39.

Miller, J. J., M. Maher, E. Bohaboy, C. S. Friedman, and P. McElhany, 2016: Exposure to low pH reduces survival and delays development in early life stages of Dungeness crab (*Cancer magister*). *Mar. Biol.*, **163** (5), 1–11, https://doi.org/10.1007/s00227-016-2883-1.

Moore, A. M., M. G. Jacox, W. J. Crawford, B. Laughlin, C. A. Edwards, and J. Fiechter, 2017: The impact of the ocean observing system on estimates of the California Current circulation spanning three decades. *Prog. Oceanogr.*, **156**, 41–60, https://doi.org/10.1016/j.pocean.2017.05.009.

Nam, S., Y. Takeshita, C. A. Frieder, T. Martz, and J. Ballard, 2015: Seasonal advection of Pacific equatorial water alters oxygen and pH in the Southern California Bight. *J. Geophys. Res. Oceans*, **120**, 5387, https://doi.org/10.1002/2015JC010859.

Newton, J. A., R. A. Feely, E. B. Jewett, P. Williamson, and J. Mathis, 2014: Global Ocean Acidification Observing Network: Requirements and governance plan. GOA-ON, 47 pp., https://www.pmel.noaa.gov/co2/GOA-ON/GOA-ON_Plan_v1.0_April2014.doc.

Nicholson, D. P., and M. L. Feen, 2017: Air calibration of an oxygen optode on an underwater glider. *Limnol. Oceanogr. Methods*, **15**, 495–502, https://doi.org/10.1002/lom3.10177.

Ohman, M. D., and Coauthors, 2013: Autonomous ocean measurements in the California Current ecosystem. *Oceanography*, **26**, 18–25, https://doi.org/10.5670/oceanog.2013.41.

——, R. E. Davis, J. T. Sherman, K. R. Grindley, B. M. Whitmore, C. F. Nickels, and J. S. Ellen, 2019: Zooglider: An autonomous vehicle for optical and acoustic sensing of zooplankton. *Limnol. Oceanogr. Methods*, **17**, 69–86, https://doi.org/10.1002/lom3.10301.

Osborne, E. B., R. C. Thunell, N. Gruber, R. A. Feely, and C. R. Benitez-Nelson, 2020: Decadal variability in twentieth-century ocean acidification in the California Current ecosystem. *Nat. Geosci.*, **13**, 43–49, https://doi.org/10.1038/s41561-019-0499-z.

Pasmans, I., A. L. Kurapov, J. A. Barth, A. Ignatov, P. M. Kosro, and R. K. Shearman, 2019: Why gliders appreciate good company: Glider assimilation in the Oregon-Washington coastal ocean 4DVAR system with and without surface observations. *J. Geophys. Res. Oceans*, **124**, 750–772, https://doi.org/10.1029/2018JC014230.

Patsavas, M. C., R. H. Byrne, R. Wanninkhof, R. A. Feely, and W. J. Cai, 2015: Internal consistency of marine carbonate system measurements and assessments of aragonite saturation state: Insights from two U.S. coastal cruises. *Mar. Chem.*, **176**, 9–20, https://doi.org/10.1016/j.marchem.2015.06.022.

Pierce, S. D., J. A. Barth, R. K. Shearman, and A. Y. Erofeev, 2012: Declining oxygen in the northeast Pacific. *J. Phys. Oceanogr.*, **42**, 495–501, https://doi.org/10.1175/JPO-D-11-0170.1.

Plant, J. N., K. S. Johnson, C. M. Sakamoto, H. W. Jannasch, L. J. Coletti, S. C. Riser, and D. D. Swift, 2016: Net community production at Ocean Station Papa observed with nitrate and oxygen sensors on profiling floats. *Global Biogeochem. Cycles*, **30**, 859–879, https://doi.org/10.1002/2015GB005349.

Rudnick, D. L., 2016: Ocean research enabled by underwater gliders. *Annu. Rev. Mar. Sci.*, **8**, 519–541, https://doi.org/10.1146/annurev-marine-122414-033913.

——, and S. T. Cole, 2011: On sampling the ocean using underwater gliders. *J. Geophys. Res. Oceans*, **116**, C08010, https://doi.org/10.1029/2010JC006849.

——, K. D. Zaba, R. E. Todd, and R. E. Davis, 2017: A climatology of the California Current System from a network of underwater gliders. *Prog. Oceanogr.*, **154**, 64–106, https://doi.org/10.1016/j.pocean.2017.03.002.

Saba, G. K., and Coauthors, 2019: The development and validation of a profiling glider deep ISFET-based pH sensor for high resolution observations of coastal and ocean acidification. *Front. Mar. Sci.*, **6**, 1–17, https://doi.org/10.3389/fmars.2019.00664.

Sherman, J., R. E. Davis, W. B. Owens, and J. Valdes, 2001: The autonomous underwater glider "Spray." *IEEE J. Oceanic Eng.*, **26**, 437–446, https://doi.org/10.1109/48.972076.

Shitashima, K., 2010: Evolution of compact electrochemical in-situ pH-pCO2 sensor using ISFET-pH electrode. *OCEANS 2010 MTS/IEEE SEATTLE*, Seattle, WA, IEEE, 1–4, https://doi.org/10.1109/OCEANS.2010.5663782.

——, Y. Maeda, and T. Ohsumi, 2013: Development of detection and monitoring techniques of CO_2 leakage from seafloor in sub-seabed CO_2 storage. *Appl. Geochem.*, **30**, 114–124, https://doi.org/10.1016/j.apgeochem.2012.08.001.

Takeshita, Y., T. R. Martz, K. S. Johnson, J. N. Plant, D. Gilbert, S. C. Riser, C. Neill, and B. Tilbrook, 2013: A climatology-based quality control procedure for profiling float oxygen data. *J. Geophys. Res. Oceans*, **118**, 5640–5650, https://doi.org/10.1002/jgrc.20399.

——, and Coauthors, 2015: Including high-frequency variability in coastal ocean acidification projections. *Biogeosciences*, **12**, 5853–5870, https://doi.org/10.5194/bg-12-5853-2015.

——, T. R. Martz, L. J. Coletti, A. G. Dickson, H. W. Jannasch, and K. S. Johnson, 2017: The effects of pressure on pH of Tris buffer in synthetic seawater. *Mar. Chem.*, **188**, 1–5, https://doi.org/10.1016/j.marchem.2016.11.002.

——, K. S. Johnson, T. R. Martz, J. N. Plant, and J. Sarmiento, 2018: Assessment of autonomous pH measurements for determining surface seawater partial pressure of CO_2. *J. Geophys. Res. Ocean*, 2–36, https://doi.org/10.1029/2017JC013387.

——, ——, L. J. Coletti, H. W. Jannasch, P. M. Walz, and J. K. Warren, 2020: Assessment of pH dependent errors in spectrophotometric pH measurements of seawater. *Mar. Chem.*, **223**, 103801, https://doi.org/10.1016/j.marchem.2020.103801.

Brought to you by NOAA Central Library | Unauthenticated | Downloaded 08/13/24 07:32 PM UTC

Testor, P., and Coauthors, 2019: OceanGliders: A component of the integrated GOOS. *Front. Mar. Sci.*, **6**, 1–32, https://doi.org/10.3389/fmars.2019.00422.

Thomson, R. E., and M. V. Krassovski, 2010: Poleward reach of the California Undercurrent extension. *J. Geophys. Res.*, **115**, C09027, https://doi.org/10.1029/2010JC006280.

Thyng, K. M., C. A. Greene, R. D. Hetland, H. M. Zimmerle, and S. F. DiMarco, 2016: True colors of oceanography. *Oceanography*, **29**, 9–13, https://doi.org/10.5670/oceanog.2016.66.

van Heuven, S., D. Pierrot, J. W. B. Rae, E. Lewis, and D. W. Wallace, 2011: MATLAB program developed for CO2 system calculations. ORNL/CDIAC-105b, Carbon Dioxide Information Analysis Center, Oak Ridge National Laboratory, accessed 11 December 2016, https://cdiac.ess-dive.lbl.gov/ftp/co2sys/CO2SYS_calc_MATLAB_v1.1/.

Vincent, A. G., R. W. Pascal, A. D. Beaton, J. Walk, J. E. Hopkins, E. M. S. Woodward, M. Mowlem, and M. C. Lohan, 2018: Nitrate drawdown during a shelf sea spring bloom revealed using a novel microfluidic in situ chemical sensor deployed within an autonomous underwater glider. *Mar. Chem.*, **205**, 29–36, https://doi.org/10.1016/j.marchem.2018.07.005.

Williams, N. L., and Coauthors, 2016: Empirical algorithms to estimate water column pH in the Southern Ocean. *Geophys. Res. Lett.*, **43**, 3415–3422, https://doi.org/10.1002/2016GL068539.

——, and Coauthors, 2017: Calculating surface ocean pCO_2 from biogeochemical Argo floats equipped with pH: An uncertainty analysis. *Global Biogeochem. Cycles*, **31**, 591–604, https://doi.org/10.1002/2016GB005541.

——, L. W. Juranek, R. A. Feely, J. L. Russell, K. S. Johnson, and B. Hales, 2018: Assessment of the carbonate chemistry seasonal cycles in the Southern Ocean from persistent observational platforms. *J. Geophys. Res. Oceans*, **123**, 4833–4852, https://doi.org/10.1029/2017JC012917.

Zaba, K. D., and D. L. Rudnick, 2016: The 2014–2015 warming anomaly in the Southern California Current System observed by underwater gliders. *Geophys. Res. Lett.*, **43**, 1241–1248, https://doi.org/10.1002/2015GL067550.

Brought to you by NOAA Central Library | Unauthenticated | Downloaded 08/13/24 07:32 PM UTC